Novel *In Situ* Synthesis in the Preparation of Ultraviolet-Curable Nanocomposite Barrier Coatings

Erin Pavlacky, Neena Ravindran, Dean C. Webster

Department of Coatings and Polymeric Materials, North Dakota State University, Fargo, North Dakota 58108

Received 7 October 2011; accepted 21 December 2011
DOI 10.1002/app.36716
Published online in Wiley Online Library (wileyonlinelibrary.com).

ABSTRACT: Ultraviolet-curable nanocomposites containing organically modified nanoclays were prepared to serve as barrier coatings against oxygen and water permeation. A novel *in situ* synthesis technique was used to produce well-dispersed clays in an unsaturated polyester polymer before crosslinking. The *in situ* dispersion route was compared with nanocomposites prepared by mixing and sonication for several levels of nanoclay loading (1, 2, 5, and 10 wt %). The comparison of nanocomposite properties prepared from each processing method demonstrated that the *in situ* preparation technique led to better clay dispersion as verified by transmission electron microscopy. The *in situ* route for nanoclay dispersion produced nanocomposites with lower water vapor transmission and permeability compared with the sonicated dispersion method. The impact on cure characteristics, mechanical properties, thermal stability, and optical clarity of the nanocomposites were also compared. © 2012 Wiley Periodicals, Inc. J Appl Polym Sci 000: 000–000, 2012

Key words: nanocomposite; clay; photopolymerization; barrier; gas permeation

INTRODUCTION

Recently, polymer/clay nanocomposites have received increased attention due to the dramatic improvements in material properties obtained with the addition of small levels of nanoclay (1–5 wt %). The improved properties include increased thermal stability,[1–3] high moduli and mechanical strength,[4] flame retardancy,[5] and decreased gas and water vapor permeability (WVP).[6,7] The enhanced properties are often attributed to the extremely high surface area interaction between the nanoclays and the polymer matrix. With average aspect ratios ranging from 10 to 1000, the incorporation of small nanoclay quantities into a polymer matrix can produce higher filler/polymer interactions than conventional composites. Additional benefits over traditional, micron-sized composite fillers include reduced weight and cost due to lower levels of nanoclay loading. Therefore, polymer/clay nanocomposites are attractive materials to study based on these significant advantages.

Montmorillonite clays are commonly incorporated into polymer matrices for improved material properties. These clays are composed of two tetrahedral silicon layers fused to an aluminum octahedral layer. The average layered silicate thickness is $\sim$ 1 nm, whereas the lateral dimension may reach several microns.[8] Exchangeable alkaline cations, such as sodium, are found in between the nanoclay layers, referred to as the gallery or interlayer. Pristine layered silicates tend to agglomerate within a polymer matrix due to the incompatibility between the inorganic-based filler and the organic polymeric material.[9] Clay surfaces must be converted into an organophilic material to facilitate their interaction with most polymer matrices. Quaternary alkylammonium salts are commonly used to render the nanoclay organophilic by undergoing an ion-exchange reaction to replace the exchangeable cations in the clay interlayer. The organic modifier selected may aid in the dispersion of the clays into polymer matrices by increasing the interlayer distance between the clay platelets. Due to the electrostatic interaction between the silicate surfaces and counterions, clays will preferentially adopt a face-to-face stacked structure.[10]

Nanocomposites may be classified based on their morphology into three distinct states of dispersion: phase-separated, intercalated, and exfoliated. With phase-separated nanocomposites, clay tactoids are formed throughout the matrix; polymer chains surround nanoclay platelets but do not penetrate between the clay layers.[11] The lack of platelet separation may result in large, micron-sized agglomerates. Intercalated nanocomposites are characterized by well-ordered nanoclay layers with polymer chains diffusing into the galleries. Due to the penetration of

Correspondence to: D. C. Webster (dean.webster@ndsu.edu).

Contract grant sponsor: ND EPSCoR; contract grant number: EPS-0814442

polymer chains, the spacing between individual clay platelets will increase, but the overall order of the clay layers is maintained. In exfoliated nanocomposites, the clay layers are dispersed individually within the continuous polymer matrix. Exfoliated nanocomposite morphology produces the highest surface area interaction between the nanoclay platelets and polymer matrix, often resulting in the most dramatic increases in physical and mechanical properties.[12] However, exfoliated morphologies are the most difficult to achieve due to the preferential parallel stacking of the nanoclays (The selection of the organic modifier is key to achieving a well-dispersed morphology).

Polymer/clay nanocomposites have been widely reported to increase the barrier properties in polymeric systems; several studies have demonstrated significant decreases in both oxygen and moisture permeability with the introduction of clay fillers into polymer matrices.[13–21] With the incorporation of impermeable clay platelets, the tortuous diffusion path principle may be applied. By greatly increasing the diffusion path of gaseous molecules and water vapor, an improvement in barrier properties may be observed. Clay volume fraction, aspect ratio, and orientation within the polymer matrix will impact the final permeation properties of polymer/clay nanocomposites.[22] Osman et al.[23] reported a decrease in oxygen gas permeability with an increase in clay volume fraction. Epoxy and polyurethane-based nanocomposites demonstrated an exponential decrease in permeability with increasing filler volume fraction. The clay filler aspect ratio will directly influence the final permeability of nanocomposite systems. In accordance with permeability models, an increased organoclay aspect ratio will ultimately increase barrier properties.[24]

The dispersion of the clay fillers within the polymer matrix is important to achieve increased barrier protection; therefore, the process selected for clay dispersion is critical to aid in the intercalation and exfoliation of the clay platelets. *In situ* intercalative polymerization techniques in the production of polymer/clay nanocomposites use polymerization reactions to produce delaminated clay platelets.[25,26] With these *in situ* techniques, the clay is swollen with a suitable liquid monomer or monomer solution before polymerization. The onset of the polymerization reaction, initiated by radiation or heat, can produce polymer chains within the clay gallery, increase the *d*-spacing between clay layers, and potentially force delamination. The implementation of an *in situ* polymerization process was first reported with polyamide nanocomposites.[27] *In situ* polymerization techniques have been reported to yield exfoliated polyethylene terephthalate (PET) nanocomposites to serve as gas barrier coatings.[28] The production of these PET nanocomposites proceeds through an *in situ* polymerization mechanism, where clay platelets delamination is initiated by PET oligomers. With continued polycondensation, exfoliated clay platelets are further separated within the polymer matrix. By using this *in situ* polymerization technique, exfoliated PET nanocomposites were produced with significant reductions in oxygen gas permeability. Katoch and Kundu[29] have also reported the production of unsaturated polyester-styrene based nanocomposites through an *in situ* type polymerization. By introducing the organoclay simultaneously with the monomers, nanocomposites with mixed intercalated/exfoliated morphologies were produced.

Ultraviolet (UV)-curing technology offers many significant advantages over traditional thermal curing including decreased cure time, low-temperature cure, and low to zero volatile emissions. UV-curable nanocomposites were first reported by Zahouily et al.[30,31] Real-time infrared spectroscopy (RTIR) and X-ray diffraction (XRD) were used to detect the formation of nanocomposites by quantifying increased spacing between nanoclay layers.[32] The influence of the organic modifier on cure characteristics, thermal stability, and mechanical properties of radiation-curable nanocomposites has also been reported.[33–35] With regards to UV-curing coatings technologies, donor-acceptor chemistry has been reported as a feasible alternative to acrylate-based systems. With donor-acceptor chemistry, free-radical induced alternating photocopolymerization is achieved by mixing an electron-deficient vinyl group with an electron-rich vinyl group.[36] The benefits of using donor-acceptor chemistry include high flexibility in polymer backbone design, low toxicity of monomers, and comparable cure times to acrylate systems. UV-curable coatings and polymer/clay nanocomposite systems based on maleate-vinyl ether donor-acceptor chemistry has previously been reported.[37,38] Maleic anhydride was used as a monomer in the synthesis of unsaturated polyester resins. These resins were subsequently photocopolymerized with vinyl ether-based reactive diluents to create UV-curable donor-acceptor coatings systems. The composition of the polymer backbone as well as the type and weight loading of clay were found to greatly influence the properties of the final radiation-curable coatings system. The organomodified clay had been incorporated into the formulation before curing using sonication; the morphology of the nanocomposites prepared with donor-acceptor chemistry was classified as intercalated. Additionally, Kim et al.[39] reported the preparation of UV-curable unsaturated polyester-styrene/clay nanocomposites through a technique of mixing a polyester resin with montmorillonite clay at high shear. Improvements in the dielectric and mechanical properties were observed

TABLE I
Unsaturated Polyester Composition

Monomer	Maleic anhydride	Diethylene glycol	1,6-hexanediol	1,4-CHDA
Moles	1.000	0.824	0.625	0.172
Weight (g)	40.96	35.99	30.41	12.41

due to clay inclusion, but XRD indicated exfoliation was not achieved as a result of clay aggregation.

The focus of this research is the development of a novel and facile *in situ* preparation technique to aid in the production of high-performance, UV-curable nanocomposite coatings and to investigate their thermal, mechanical, and barrier properties. Although *in situ* processes have been reported previously to produce nanocomposite films, much of the focus has been on implementing these *in situ* techniques in thermoplastic polymer systems. With a desire to prepare UV-cured nanocomposite films having a high degree of nanoclay dispersion, we have explored the use of a novel *in situ* synthesis method to enable the dispersion and subsequent delamination of clay platelets in a polyester resin precursor, followed by crosslinking using donor-acceptor chemistry. Therefore, the degree of clay exfoliation is already achieved before UV-curing. The objective of this study is to implement a novel *in situ* preparation process and examine the impact of clay loading and functionalization on the ability to produce exfoliated UV-curable nanocomposite barrier films and to further explore the impact of clay incorporation on physical and mechanical properties.

EXPERIMENTAL

Materials

Monomers purchased from Sigma Aldrich (Milwaukee, WI) for unsaturated polyester synthesis were maleic anhydride, 1,6-hexanediol, and diethylene glycol. Monomer 1,4-cyclohexanedicarboxylic acid (1,4-CHDA) was obtained from Eastman Chemical Company (Kingsport, TN). Reactive diluent triethyleneglycol divinyl ether (TEGDVE) was obtained from BASF (Ludwigshagen, Germany). Photoinitiator, 2-hydroxy-2-methyl-1-phenyl-propan-1-one (Darocur® 1173) was supplied by CIBA (Basel, Germany). Cloisite® Na^+, a natural unmodified montmorillonite clay (cation exchange capacity, CEC = 92 meq/100 g), and Cloisite® 30B, a natural montmorillonite clay modified with methyl tallow bis-2-hydroxyethyl ammonium cations (CEC = 90 meq/100 g), were obtained from Southern Clay Products (Gonzales, TX). The organic modifier cetyltrimethylammonium bromide (CTAB) was also purchased from Sigma Aldrich. All chemicals were used as received without further purification.

Preparation of clays

CTAB-modified nanoclays were prepared through an ion exchange reaction between unmodified montmorillonite clay Cloisite® Na^+ and alkylammonium surfactant CTAB. A total of 5.00 g of CTAB were added to 200 mL of deionized water in a reaction flask equipped with stirrer and temperature controller. The CTAB-H_2O solution was heated to 50°C for 2 h under constant stirring. A total of 1.50 g of Cloisite® Na^+ was added to the solution and stirred for 24 h at 50°C. The CTAB-modified clay was centrifuged for 15 min at 5000 RPM, filtered with deionizied water and ethanol to remove excess bromine, dried in an oven, and ground using a mortar and pestle. The resulting clay is hereafter referred to as CTAB-modified clay. Cloisite® 30B was used without further modification.

Synthesis of unsaturated polyester via *in situ* technique

Unsaturated polyesters were prepared by standard melt polyesterification. The unsaturated polyester composition is indicated in Table I. The clay was first added to the liquid monomer diethylene glycol based on the desired loading of the final nanocomposite (1, 2, 5, and 10 wt %). The diethylene glycol and clay mixture was dispersed at high shear, and then mixed via magnetic stir bar overnight. The diethylene glycol/clay dispersion and remaining monomers were weighed into a 250 mL, three-necked, round bottom flask equipped with nitrogen inlet, condenser, mechanical stirrer, temperature controller, and heating mantle. The polyester synthesis was conducted in a nitrogen atmosphere to prevent oxidation of the double bonds and other side reactions. The reaction was ramped in a controlled manner to 60°C, 120°C, and 180°C. Water was collected from the polyester synthesis as the polymerization proceeded. The polyester reaction was stopped when an acid number $\sim$ 20 mg of KOH/g of sample was achieved. A control unsaturated polyester was synthesized without clay.

Unsaturated polyester/clay dispersion via sonication technique

Unsaturated polyester containing no clay, hereafter referred to as the control polyester, was mixed with Cloisite® 30B clay and sonicated for 8 h using an

ultrasonic bath to compare the sonication technique of clay dispersion to the *in situ* process.

Preparation of nanocomposites

Nanocomposites were prepared by mixing the unsaturated polyester sample and reactive diluent TEGDVE at a 1 : 1 stoichiometric ratio based on reactive functional groups: maleate to vinyl ether. Photoinitator Darocur® 1173 was added at 6 wt % based on total polyester, reactive diluent, and clay. The nanocomposite formulations were mixed for uniformity, and then left undisturbed for 2 h to remove air bubbles. Next, samples were cast on glass and aluminum substrates with a Gardco bar-coater at 5 mil clearance (75–85 μm dry film thickness). The cast formulations were cured under UV-light by a Dymax 200 EC silver lamp (UV-A, 365 nm, intensity $\approx$ 40 mW cm^{-2}) until the films were tack-free (60 s). Testing was performed after 24 h to allow the nanocomposite coatings to equilibrate.

Nomenclature

Because the polyester composition was kept consistent throughout each polyesterification reaction, the nomenclature for the unsaturated polyesters was designated based on clay loading, clay type, and dispersion method. The name of each polyester is as follows: wt % clay_type_dispersion method, such as 1_30B_insitu for an unsaturated polyester containing 1% Cloisite® 30B clay synthesized using the *in situ* clay dispersion method. The clay type CTAB indicates the Cloisite® Na^+ nanoclay modified with CTAB. The term "sonic" refers to clays dispersed in virgin polyester by sonication. The coatings are named based on the polyester used in its formulation, but the prefix "NC" distinguishes the nanocomposite coating from the polyester.

Characterization

The unsaturated polyesters were characterized for molecular weight, viscosity, glass transition temperature (T_g), and maleate-fumarate isomerization. Molecular weight was determined using a Waters 2410 Gel Permeation Chromatograph (GPC) equipped with a refractive index detector. Polyester was dissolved in solvent tetrahydrofuran to create a 1% sample solution and filtered by a 0.2 μm PET filter to remove any clay agglomerates. The flow rate was 1 mL min^{-1}, and calibration was performed with polystyrene standards. Viscosity measurements were made with an ICI cone and plate viscometer at 100°C. The T_g was determined from differential scanning calorimetry (DSC) using a TA Instruments Q1000 Series DSC. The test method was a heat-cool-heat cycle. Polyester samples were equilibrated at −90°C, heated to 100°C at a rate of 10°C min^{-1}, cooled to −90°C at a rate of 10°C min^{-1}, then heated once again to 100°C at a rate of 10°C min^{-1}. T_g values were determined from the inflection point in the second heating scan. The isomerization from maleate to fumarate in the unsaturated polyester backbone was determined from ^1H nuclear magnetic resonance (NMR) spectroscopy using a JEOL ECA Series 400 MHz NMR spectrometer with procedure followed from Curtis et al.[40]

The cure characteristics were determined using a Thermo Nicolet Magna-IR 850 spectrometer with detector type DTGS KBr to perform RTIR measurements. A LESCO Super Spot MK II UV-curing lamp equipped with a fiber-optic light guide was UV-irradiation source for curing the samples. The formulations were spin-coated at 3000 RPM onto a KBr window, placed into the spectrometer chamber, and subjected to UV and IR irradiation simultaneously. The samples were $\sim$ 20 mm from the end of the fiber-optic cable with a light intensity of 10 mW cm^{-2}. The degree of conversion was determined from the disappearance of the vinyl ether double bonds (1639 cm^{-1}). The conversion was calculated from

$$\% \text{ conversion} = \{[(A_{1639})_0 - (A_{1639})_t]/(A_{1639})_0\} \times 100$$

where $(A_{1639})_0$ is the absorbance at time = 0 and $(A_{1639})_t$ is the absorbance at time = t.

Nanocomposite morphology was characterized by XRD and transmission electron microscope (TEM). X-ray powder diffraction was collected using a Bruker AXS' D8 Discover diffractometer in Bragg-Brentano geometry, using Cu Kα radiation with a wavelength of 1.5406 Å. The samples were scanned from 1.5°– 50° 2θ, using a step size of 0.02° 2θ and a run time of 1 s/step. Samples for TEM were thin cut using a diamond knife and RMC MTXL ultramicrotome. The thin sections were placed on 400 mesh copper grids and photographed using a JEOL 100 cx-II TEM operating at 80 kV. Water vapor transmission (WVT) testing was performed in accordance with ASTM E96, "Standard Test Methods for Water Vapor Transmission of Materials," by the Water Method. A controlled humidity chamber was used to maintain relative humidity at 70% ± 2% and 20°C ± 2°C. Under steady state conditions, the mass loss over time correlated with WVT and permeance. Duplicate samples were performed to verify results. Oxygen gas permeability measurements were conducted with a MOCON Oxtran 2/21 Oxygen Permeability Instrument (Modern Control, Minneapolis, MN) in accordance with ASTM D3985 (0% RH, 25°C). Duplicate samples of each nanocomposite film were submitted to verify results.

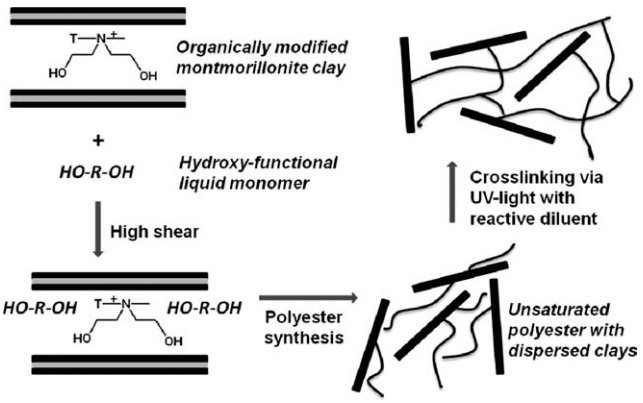

Scheme 1 Representation of *in situ* technique leading to exfoliated nanoclay platelets (T = tallow).

The dynamic mechanical properties were tested using a TA Instruments Q800 Dynamic Mechanical Analyzer in tensile mode. Free films of the cured coatings ~ 15 mm length, 5 mm width, and 0.070–0.078 mm thickness were characterized using 1 Hz frequency, constant strain of 0.05%, heating rate of 5°C min^{-1} over a temperature range of −50°C to 150°C. Film hardness was determined using a BYK-Gardner pendulum hardness tester on aluminum panels. Thermal stability was determined using thermogravimetric analysis (TGA) with a TA Instruments Q500 Thermogravimetric Analyzer. Cured samples were heated in nitrogen from 25°C to 800°C at a rate of 20°C min^{-1}. The optical clarity was measured with a Varian Cary 5000 UV-Vis Spectrometer by determining transmittance at 400 nm.

RESULTS AND DISCUSSION

In situ synthesis technique

In previous studies, we reported the development of UV-curable coatings and polymer/clay nanocomposites based on the nonacrylate technology of donor-acceptor chemistry.[37,38] Sonication was used to disperse the clay and monomers before photocopolymerization, and the resulting nanocomposite morphology was classified as intercalated. To further increase clay dispersion, a novel *in situ* preparation technique was explored to produce highly dispersed clays in a polymer resin before crosslinking. With this novel technique, the dispersion of nanoclays in the unsaturated polyester resins before crosslinking depends on the diffusion of liquid monomer into the nanoclay interlayers. Scheme 1 illustrates the *in situ* process for nanoclay dispersion. Initially, the nanoclay layers stack face-to-face due to favorable electrostatic interactions between the negatively charged clay platelets and exchangeable cations in the nanoclay interlayer. The interlayer space is equivalent to the organic modifier volume. By introducing a liquid monomer at high shear, the monomer may diffuse into the nanoclay interlayer. The onset of the unsaturated polyester polymerization will lead to oligomeric chain growth. The increase in volume from the growing oligomeric chains may then increase the volume between the nanoclay layers; therefore, the distance between the nanoclay layers will increase. Through this *in situ* process, it is possible to expand the interlayer spacing to produce highly dispersed nanoclays within the polyester before crosslinking. Additionally, the functionality of the nanoclay organic modifier may aid in the exfoliation process. Hydroxy-functional organic modifiers, such as the modifier for Cloisite® 30B, may react with the acid-functional monomers during polyesterification, thereby becoming incorporated into the polyester backbone and further inducing exfoliation of nanoclay platelets. The CTAB-modified clay provided an organic modification without hydroxy-functionality to explore the impact of the modifier on the final polyester and nanocomposite film properties.

Unsaturated polyester characterization

The properties of the unsaturated polyesters containing nanoclay were characterized to examine the effect of the nanoclay dispersion technique and loading. Polyester properties provide insight to the properties of the nanocomposite films. Table II is a comprehensive summary of the polyesters synthesized and their characterization. The target acid number was ~ 20 mg of KOH/g of the polyester resins. All polyester reactions were stopped once an acid number near this value was achieved. Comparable acid numbers were important in the characterization of the unsaturated polyesters as similar acid number values produce similar degrees of polymerization.[41]

The molecular weight and polydispersity of the unsaturated polyesters was determined from GPC to examine the impact of the clay. The introduction of clay into the polymer system increased the apparent molecular weight in all unsaturated polyesters. Because the clay was not removed before GPC analysis, the increases in molecular weight may be a reflection of higher hydrodynamic volumes from the polyester oligomers containing the clay fillers. The polydispersity index ranged from 1.8 to 2.7, showing higher breadth of molecular weight distribution typical of step-growth polymerizations. The relationship between nanoclay loading and viscosity demonstrated the dramatic influence of the incorporation of even small amounts of clay into a polymer system. The control polyester had a viscosity of 2.4 Poise, and the introduction of just 1 wt % clay increased the viscosity regardless of the dispersion route or clay type. Increasing the concentration of clay led to higher unsaturated polyester viscosities.

TABLE II
Unsaturated Polyester Properties

Polyester	Acid number	M_n (g mol^{-1})	M_w (g mol^{-1})	PDI	Viscosity (Poise)	T_g (°C)	% Fumarate
Control	21	1000	2200	2.2	2.4	−42	33
1_30B_insitu	21	1800	3500	1.9	3.3	−36	46
2_30B_insitu	22	1500	3800	2.5	5.4	−39	39
5_30B_insitu	21	1800	3900	2.2	5.8	−41	41
10_30B_insitu	21	4000	7300	1.8	8.8	−43	64
1_30B_sonic	21	1900	3600	1.9	3.5	−37	19
2_30B_sonic	21	2000	3600	1.8	3.7	−37	17
5_30B_sonic	21	1400	3500	2.4	4.8	−41	24
10_30B_sonic	21	1900	3800	2.0	5.4	−42	18
1_CTAB_insitu	20	2800	6900	2.4	6.0	−32	53
2_CTAB_insitu	21	2400	4700	2.0	6.5	−33	62
5_CTAB_insitu	22	1800	4800	2.7	7.3	−36	52

A direct trend between clay loading and viscosity was apparent with higher clay loadings resulting in higher viscosities. The unsaturated polyesters synthesized with CTAB-modified clay had slightly higher viscosities compared with the Cloisite® 30B at the same clay loading, most likely a consequence of poorer compatibility between the CTAB-modified clay and polyester oligomers. The Cloisite® 30B-containing polyesters prepared through the *in situ* preparation technique were higher in viscosity than those dispersed through sonication for the same clay loading. The glass transition temperatures (T_g) of these unsaturated polyesters showed an interesting trend with increasing the clay content. The addition of small levels of nanoclay (1 or 2 wt %) increased the T_g slightly, up to 10°C higher than the control polyester, but higher clay amounts (5 and 10 wt %) barely affected the T_g. The small T_g changes observed with clay inclusion into the polyester resin may be a result of the low molecular weight polyester oligomers. Additionally, the control unsaturated polyester resin has a relatively low T_g (−42°C), so the impact of clay on the polyester T_g may not be as dramatic as polymers with higher T_g values.

The variables influencing maleate-fumarate isomerization have been studied in unsaturated polyesters, where the reaction environment, monomers, and catalyst all affect the final degree of isomerization.[42] Polyesters synthesized from maleic anhydride often exhibit reactivity similar to polyesters synthesized from fumaric acid, a trend attributed to the conversion of maleic to fumaric unsaturation during polyesterification.[40] Polyesters exhibiting cis–trans conversion along its backbone have also exhibited higher hardness and chemical resistance. The isomerization of the unsaturated polyester backbone from maleate to fumarate was found to be greatest with the polyesters synthesized by the *in situ* technique. Curtis et al.[40] have reported the preference of hydroxyl-functional monomers to react with the trans isomer in polyesterification reactions when the hydroxyl groups are sterically hindered. Additionally, when the monomers exhibit less steric hindrance, the preference of reacting with the cis or trans isomer decreases. The dispersion of the nanoclays may greatly influence the final degree of isomerization. If the *in situ* technique increased clay dispersion, the trans-fumarate isomerization may be promoted as the fumarate isomerization is less influenced by steric effects.[43] The preference to react with the trans isomer is reflected by higher values of fumarate isomerization compared with the control unsaturated polyester.

Cure characteristics

Higher conversion with UV-irradiation was observed in every nanocomposite formulation compared with the control sample containing no clay filler. The extent of the reaction was monitored by the disappearance of the vinyl ether double bond (1639 cm^{-1}), indicating the degree of conversion based on donor-acceptor chemistry of the maleate-vinyl ether coatings system. The control sample had a conversion of 72%, whereas each nanocomposite formulation resulted in conversions ranging from 80% to 87% (Fig. 1). The increased conversion achieved with the addition of clay fillers is attributed to the viscosity of the nanocomposite formulations. As seen in Table II, the viscosities of the unsaturated polyesters containing clay had significantly greater viscosities than that of the control polyester. Higher viscosities may result in an autoacceleration effect. With the increased viscosity, it becomes more difficult for chain ends bearing radicals to diffuse through the system, thus decreasing the rate of termination. The lower molecular weight reactive diluent and oligomers may more easily diffuse through the system leading to increased conversion. Similar trends regarding increased conversion with the introduction of clay has been reported in other UV-curable nanocomposite systems.[33,38,44]

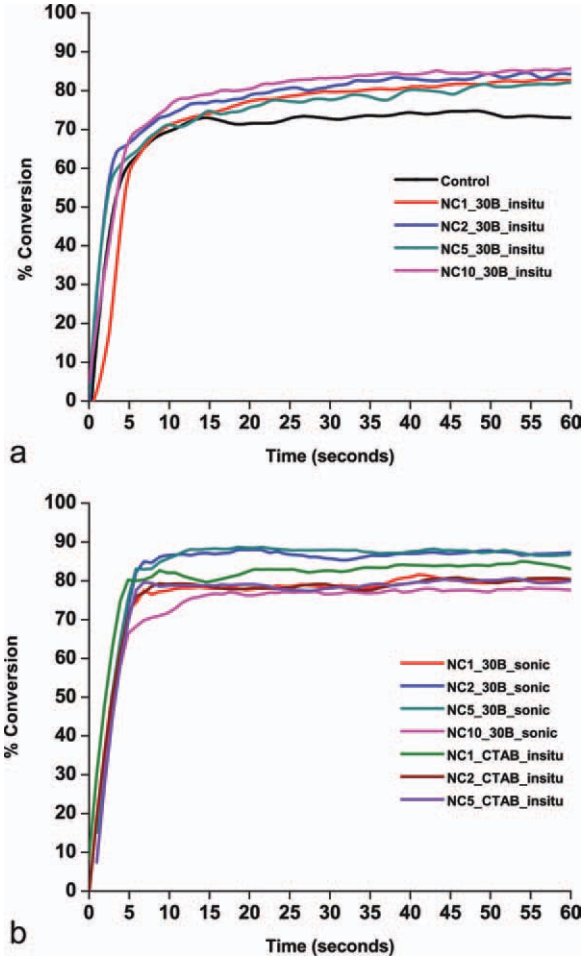

Figure 1 RTIR conversions of the vinyl ether double bond (1639 cm^{-1}) with (a) *in situ* nanocomposite formulations and (b) sonicated and CTAB-modified clay nanocomposite formulations with 60 s of UV exposure [Color figure can be viewed in the online issue, which is available at wileyonlinelibrary.com.]

Nanocomposite morphology

With the *in situ* technique to incorporate nanoclays, increased nanoclay delamination may occur as a result of the growing oligomeric polyester chains occupying more volume within the gallery. Increasing the distance between the nanoclay layers leads to a high degree of dispersion within the polymer system. After the unsaturated polyesters are crosslinked by reactive diluent TEGDVE, an exfoliated nanocomposite may be formed. Because the final degree of clay dispersion cannot be changed once curing has occurred, delamination of the clay before crosslinking is critical to aiding the exfoliation process. The morphology of the UV-curable nanocomposite films has a profound impact on the final coating properties. The degree of dispersion will dictate the extent of polymer-nanoclay surface area interaction with high levels of dispersion leading to the greatest surface area interaction. Therefore, nanocomposite morphology determination is crucial to the explanation of film properties.

Two techniques have been used to characterize nanocomposite morphology: XRD and TEM. XRD was conducted to determine the *d*-spacing, or distance of the nanoclay interlayer, of the resulting nanocomposite films. An increase in the *d*-spacing indicates the intercalation of polymer between nanoclay platelets, thus, the formation of nanocomposites. Figure 2 displays the XRD patterns of the pristine clays as well as the nanocomposite coatings. Two prominent diffraction peaks were observed at 4.78 and 4.12 2θ for Cloisite® 30B and the CTAB-modified clay, respectively. Using Bragg's Law, the interlayer spacing for Cloisite® 30B was 1.85 and 2.14 nm for the CTAB-modified clay. In stark contrast to the distinct clay diffraction peaks, each nanocomposite film had an absence of any prominent peaks at low 2θ angles. This absence of peaks may indicate the formation of exfoliated nanocomposite morphologies as the clay

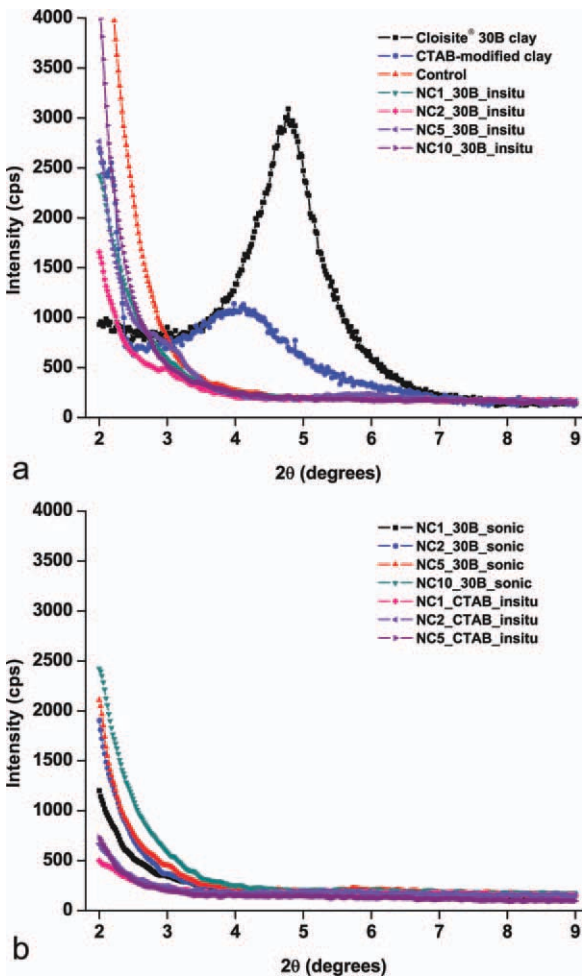

Figure 2 XRD patterns of (a) pristine Cloisite® 30B, CTAB-modified clay, and *in situ* prepared nanocomposite films, and (b) sonicated and CTAB-modified clay containing nanocomposite films [Color figure can be viewed in the online issue, which is available at wileyonlinelibrary.com.]

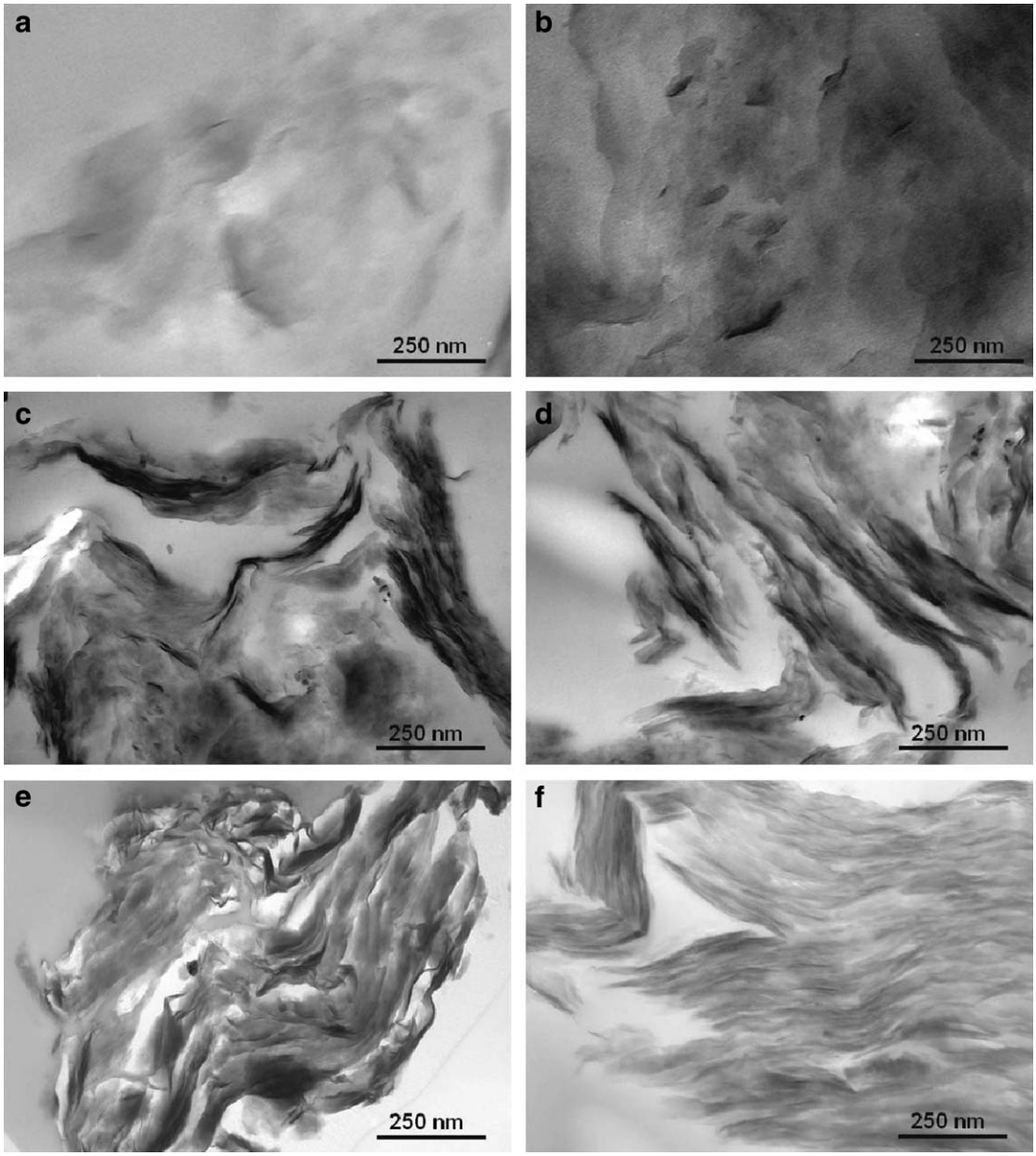

Figure 3 TEM micrographs of (a) NC1_30B_insitu, (b) NC2_30B_insitu, (c) NC5_30B_insitu, (d) NC10_30B_insitu, (e) NC5_30B_sonic, and (f) NC1_CTAB_insitu.

platelets have been delaminated to a high enough degree to become disoriented and unable to produce diffraction with wide-angle XRD techniques.[45] Although XRD is widely reported to classify polymer/clay nanocomposite morphology, the absence of peaks may also be an indication of poor calibration or clay orientation. Furthermore, low levels of clay loading may fail to produce a Bragg diffraction peak.[46]

Although the absence of peaks from the nanocomposite XRD patterns was a promising indicator for high clay dispersion, TEM was an important and necessary technique to more accurately characterize nanocomposite morphology. TEM micrographs (Fig. 3) of the nanocomposite samples indicate that the *in situ* preparation technique produced exfoliated nanocomposites at 1 and 2 wt % and mostly intercalated at 5 and 10 wt %. At the lower levels of clay loading, the clay platelets are well dispersed and randomly oriented, whereas nanocomposites NC5_30B_insitu and NC10_30B_insitu display ordered clay layers, although increased separation between clay platelets was observed. Intercalation was predominantly observed with the sonication dispersion technique; these nanocomposites did not exhibit an exfoliated morphology. The CTAB-modified clay containing nanocomposites also produced predominantly intercalated nanocomposites even with low levels of clay loading, suggesting the importance

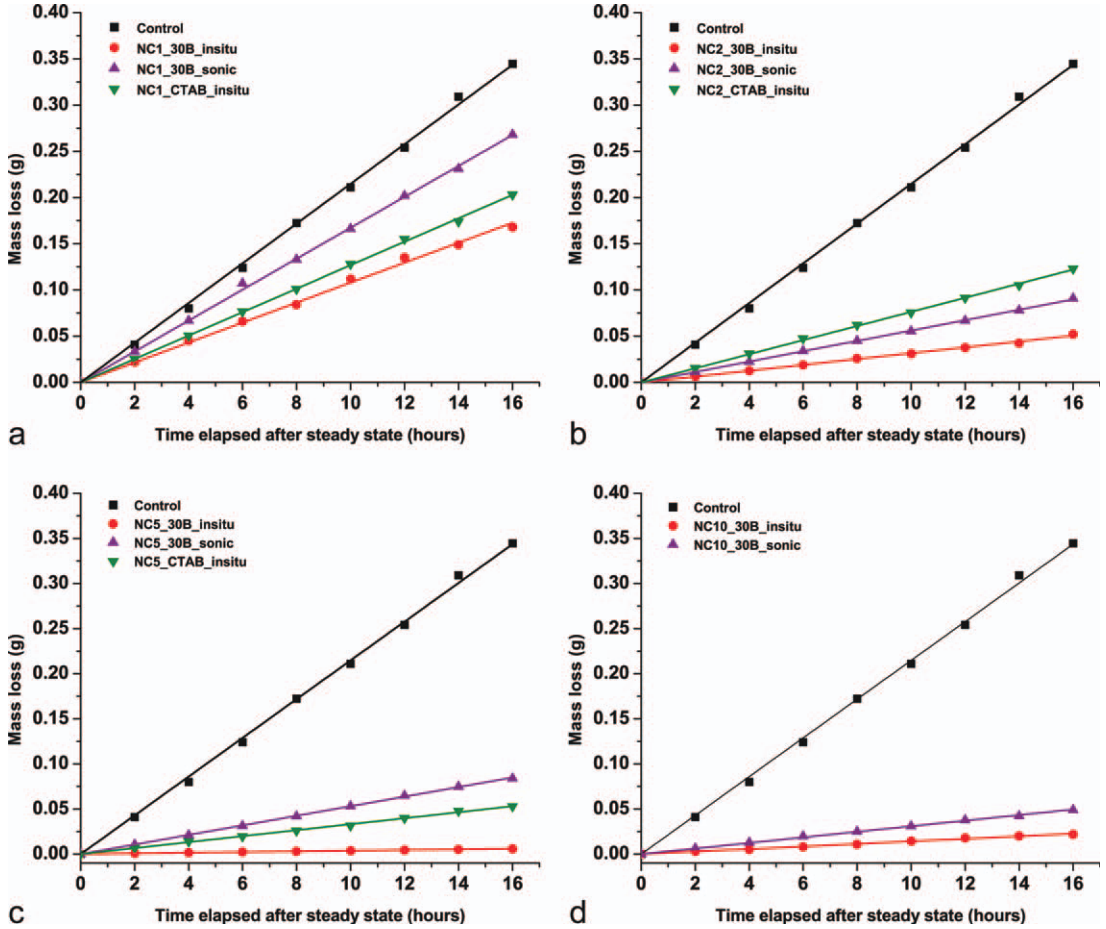

Figure 4 Mass loss over time once steady state conditions were achieved for nanocomposite films. Comparison of 1 wt % (a), 2 wt % (b), 5 wt % (c), and 10 wt % (d) displayed [Color figure can be viewed in the online issue, which is available at wileyonlinelibrary.com.]

of the hydroxyl functionality of the organic modifier to achieve exfoliation through the *in situ* technique.

Water Vapor Transmission and Permeability

The results shown in Figure 4 and the data summarized in Table III indicate the *in situ* preparation technique yielded nanocomposites with lower WVT and WVP, in accordance with ASTM E96 Water Method. Figure 4 demonstrates the superiority of the *in situ* process in nanocomposite preparation to serve as barriers compared with the sonication preparation technique and CTAB-modified clay containing nanocomposites; the *in situ* process has the lowest mass

TABLE III
Nanocomposite Water Vapor Transmission and Water Vapor Permeability

Nanocomposite	Mass loss/ time (g h^{-1})	WVT (g m^{-2} s^{-1})	Avg. film thickness (μm)	WVP (g·m $(m^2 \cdot s \cdot Pa)^{-1}$)
Control	2.15 E −02	5.97 E −03	86	8.79 E −10
NC1_30B_insitu	1.02 E −02	2.83 E −03	80	3.88 E −10
NC2_30B_insitu	3.17 E −03	8.81 E −04	83	1.25 E −10
NC5_30B_insitu	3.78 E −04	1.05 E −04	78	1.40 E −11
NC10_30B_insitu	1.41 E −03	3.92 E −04	81	5.43 E −11
NC1_30B_sonic	1.67 E −02	4.64 E −03	79	6.27 E −10
NC2_30B_sonic	5.61 E −03	1.56 E −03	84	2.24 E −10
NC5_30B_sonic	5.31 E −03	1.48 E −03	78	1.97 E −10
NC10_30B_sonic	3.09 E −03	8.58 E −04	80	1.17 E −10
NC1_CTAB_insitu	1.27 E −02	3.53 E −03	80	4.83 E −10
NC2_CTAB_insitu	7.63 E −03	2.12 E −03	78	2.83 E −10
NC5_CTAB_insitu	3.31 E −03	9.19 E −04	82	1.29 E −10

TABLE IV
Nanocomposite Oxygen Gas Permeability

Nanocomposite	OTR (cc 100 in^{-2} day^{-1})
Control	1.88
NC1_30B_insitu	1.45
NC2_30B_insitu	2.07
NC5_30B_insitu	1.73
NC10_30B_insitu	1.95

loss for every level of clay loading. Figure 4(a) demonstrates that the introduction of just 1 wt % clay reduced the mass loss of water over time. With the introduction of higher levels of clay loading, the mass loss was more significantly reduced. NC5_30B_insitu and NC10_30B_insitu had the lowest mass loss over time, which correlated into the lowest WVT and WVP of any nanocomposite sample. The performance of the *in situ* prepared nanocomposites in reducing WVT and WVP is attributed to the higher level of nanoscale dispersion of the nanoclay filler. By using the polyester polymerization to increase the spacing between nanoclay platelets, the clay filler reached a higher degree of dispersion. This dispersion was maintained with the formation of the nanocomposite coatings, resulting in nanocomposites providing a more tortuous diffusion path for water molecules. Although the *in situ* process did not create perfectly exfoliated nanocomposites with 5 and 10 wt % clay, the mass loss of water is lower than the sonicated nanocomposite films indicating that a higher degree of dispersion was achieved with the *in situ* preparation. One noteworthy example of the improvement in barrier protection provided by the *in situ* process was the level of clay needed in the *in situ* process compared with the sonication technique to provide the same level of barrier protection: NC2_30B_insitu recorded approximately the same WVT and WVP as NC10_30B_sonic. Not only did the *in situ* process produce better barrier protection but also the *in situ* nanocomposites needed significantly less clay to achieve those barrier properties.

Oxygen gas permeability

In contrast to the WVT results reported in the previous section, the *in situ* technique in the preparation of UV-curable nanocomposites did not demonstrate any concrete trends regarding oxygen gas permeability. Table IV lists the oxygen barrier results obtained from MOCON (Minneapolis, MN) for the series of *in situ* prepared nanocomposite films containing the hydroxy-functional clay, Cloisite® 30B. Although no direct correlation existed between the clay loading and the oxygen barrier properties of the nanocomposite films, these films still were in the acceptable oxygen transmission rate (OTR) range of a medium barrier layer, such as for certain food and beverage packaging materials.[47] For example, PET is a commonly used material in the packaging of juice, water, beer, meats, and cheeses. The O_2 permeability of PET films is reported to be $\sim$ 6–10 cc 100 in^{-2} day^{-1}.[48] The *in situ* prepared nanocomposites had lower OTR values than PET, ranging from 1.45–2.07 cc 100 in^{-2} day^{-1}. Unlike the trends observed with WVT, the addition of clay did not drastically lower the oxygen barrier properties of the nanocomposite samples. Several factors will influence the permeation through the films including clay size, orientation, and compatibility between the permeating species and polymer film. Larger reductions in WVT than OTR were also reported by Osman et al.[49] for polyurethane-clay nanocomposites. One explanation given for the difference in water vapor and oxygen gas permeability was the size of the permeating groups. Because water vapor molecules may form into clusters during their diffusion through polymers, the clusters may increase the diffusion time.[50] As oxygen gas molecules do not similarly form clusters during diffusion, their diffusion may proceed more readily through polymer films. Additionally, the OTR of the control coating (1.88 cc 100 in^{-2} day^{-1}) was also considered to be in the range of a medium oxygen barrier.

Mechanical and thermal properties

DMTA was used to examine the cured nanocomposite viscoelastic properties. Overall, nanocomposite films containing lower levels (1 and 2 wt %) of clay loading exhibited higher storage modulus and hardness values as well as higher degradation temperatures than nanocomposites with higher clay loading (5 and 10 wt %). A summary of these results are compiled in Table V and displayed in Figures 5–7. The storage modulus at room temperature of each

TABLE V
Mechanical and Thermal Characterization Data

Nanocomposite	E' (MPa, 25°C)	König hardness (s)	T_{10}% (°C)
Control	370	83	240
NC1_30B_insitu	890	84	255
NC2_30B_insitu	1020	93	245
NC5_30B_insitu	1250	82	250
NC10_30B_insitu	1500	76	230
NC1_30B_sonic	810	96	270
NC2_30B_sonic	910	89	290
NC5_30B_sonic	625	84	300
NC10_30B_sonic	390	71	280
NC1_CTAB_insitu	610	93	270
NC2_CTAB_insitu	495	87	280
NC5_CTAB_insitu	340	63	260

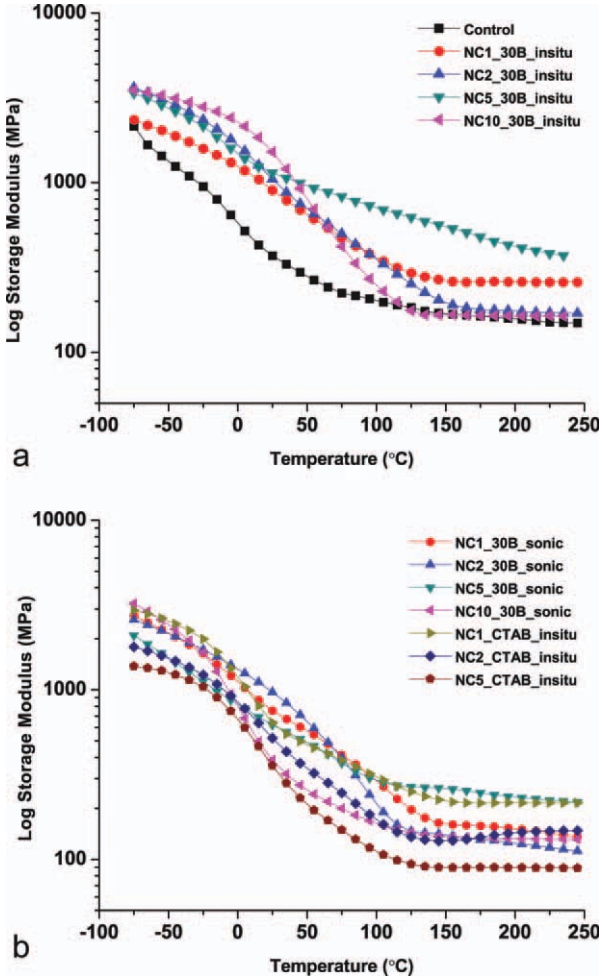

Figure 5 Storage modulus plots from DMTA for (a) *in situ* nanocomposite films and (b) sonicated and CTAB-modified clay nanocomposite films [Color figure can be viewed in the online issue, which is available at wileyonlinelibrary.com.]

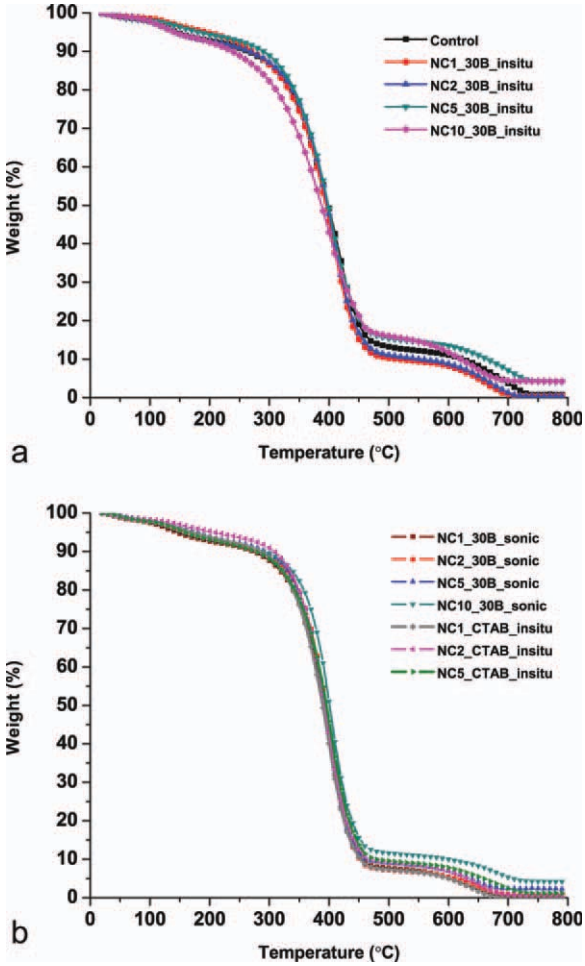

Figure 7 TGA degradation curves of the (a) *in situ* preparation nanocomposites and (b) sonication and CTAB-modified clay nanocomposites [Color figure can be viewed in the online issue, which is available at wileyonlinelibrary.com.]

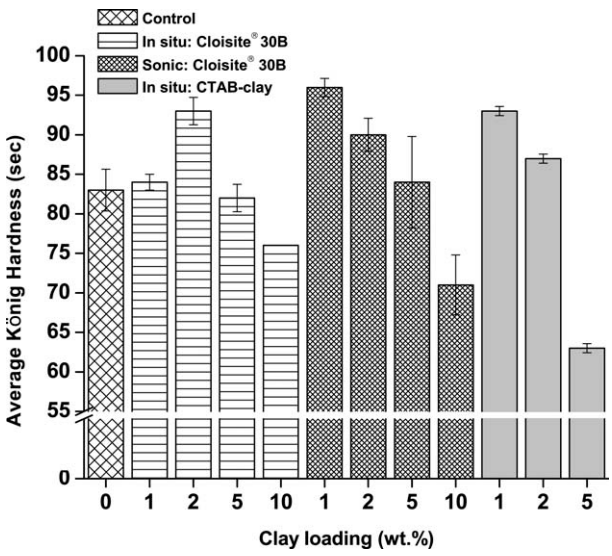

Figure 6 König pendulum hardness of the nanocomposite coatings.

nanocomposite sample was found to clearly be related to the dispersion technique and clay content. With the *in situ* preparation technique, the storage modulus was increased over 500 MPa with NC1_30B_insitu from the control coating. Further increases in the clay loading led to additional increases in the storage modulus, with NC10_30B_insitu recording a storage modulus of 1500 MPa at room temperature. In contrast, the trend of higher storage modulus values with higher levels of clay loading was not reflected with the nanocomposites containing the CTAB-modified clay or the nanocomposites based on the sonication dispersion technique. With clay loading up to 2 wt %, these nanocomposites demonstrated increased storage modulus values, but nanocomposites containing 5 and 10 wt % clay resulted in a decrease in the storage modulus. This trend is most likely a consequence of poorer clay dispersion throughout the nanocomposite film. As seen with TEM analysis, the nanocomposites prepared with the CTAB-modified clay or through the

sonication preparation technique were intercalated with portions of phase separation at higher clay loading. With phase-separated clay domains throughout the nanocomposite, the mechanical properties may diminish as the reinforcing effect of the clay fillers decreases from agglomeration. Nanocomposite NC10_30B_sonic had approximately the same storage modulus as the control coating, and nanocomposite NC5_CTAB_insitu actually had a lower storage modulus value than the control. A similar trend is observed with König pendulum hardness of the nanocomposite coatings. The nanocomposite coatings containing 1 and 2 wt % clay loading exhibited higher König hardness values than the coatings with 5 and 10 wt % clay, regardless of dispersion route (Fig. 6).

The thermal stability of the nanocomposite samples showed a similar trend as a function of clay loading: nanocomposites containing lower levels of clay loading generally had greater thermal stability. The TGA degradation curves are displayed in Figure 7, and Table V reports the temperature at 10% weight loss (T_{10}%). The control coating had a T_{10}% of 240°C; NC1_30B_insitu, NC2_30B_insitu, and NC_5_30B_insitu each had slightly higher T_{10}%, up to a 15°C increase. Conversely, NC10_30B_insitu had the lowest T_{10}% at 230°C. Increased thermal stability was also observed with each nanocomposite prepared through the sonicated technique as well as the CTAB-modified clay, particularly at 1–2 wt % clay. Again, the higher levels of clay loading seemed to diminish the improvement in thermal stability observed with low levels of clay filler.

After examining both the mechanical and thermal properties of the UV-curable nanocomposite films, a significant trend occurred: nanocomposites with lower levels of clay (1–2 wt %) demonstrated increased modulus, hardness, and thermal stability but higher levels of clay (5–10 wt %) did not continually increase the material properties. Instead, nanocomposites with higher clay loading demonstrated diminished mechanical and thermal properties, when compared with nanocomposites containing lower clay loading. Based on these results, it becomes apparent that there is a significant influence from the clay loading on the final nanocomposite mechanical properties. Miyagawa et al.[51] reported a decrease in the T_g of anhydride-cured epoxy nanocomposites with increased clay volume fraction. The explanation for this phenomenon was hypothesized to be an effect of the organic modifier plasticizing the coatings system. With increased clay amounts in the nanocomposite system, there is also an increase in the amount of the organic modifier within the cured coating. The organic modifier containing a long-chain fatty acid may act as a plasticizer, thus lowering the T_g with increased clay content. Based on trends observed with T_g, the mechanical and thermal properties of the nanocomposites may also be affected by the increased organic modifier concentration with higher levels of clay loading. Additional experimentation will be conducted to further explore this trend.

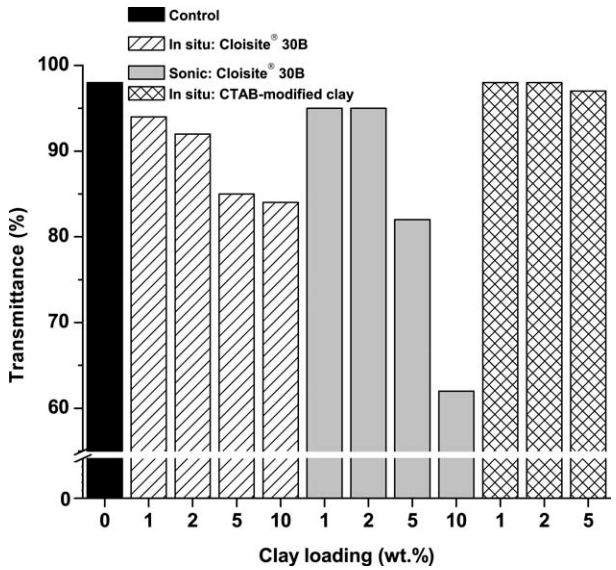

Figure 8 Transmittance of nanocomposites at 400 nm.

Optical clarity

Although low concentrations of nanoclays maintained high optical clarity, dramatic decreases in transmittance of the nanocomposite films were observed with higher levels of nanoclay loading. Nanoscale distribution of the silicate platelets contributes to the high optical clarity observed in many polymer/clay nanocomposites.[52] Figure 8 shows the transmittance at 400 nm for each nanocomposite. The control coating had high optical clarity with 98% transmittance. The contribution of 1 and 2 wt % clay, regardless of clay type of dispersion technique, decreased the optical clarity slightly (92%–97%). The clarity of these nanocomposites is a direct reflection of the low volume fraction of clay present in the sample coupled with the degree of dispersion. With increases in clay loading to 5 and 10 wt %, more dramatic decreases in the optical clarity are observed. In particular, the nanocomposites prepared through the sonication technique became much more opaque with the introduction of 5 and 10 wt % clay leading to percent transmittance values of 82% and 62%, respectively. Although the *in situ* preparation of nanocomposites also reflected a decrease in optical clarity with higher clay loadings, the transmittance was much higher than the sonication preparation. NC5_30B_insitu had 85% transmittance, and NC10_30B_insitu had a transmittance value of 84%. The higher optical

clarity of the *in situ* based nanocomposite coatings compared with the sonication technique may reflect a much greater dispersion of nanoclay fillers, as seen with TEM micrographs. Additionally, the CTAB-modified clay nanocomposites maintained high optical clarity regardless of clay loading.

CONCLUSIONS

UV-curable nanocomposite coatings were successfully prepared by a novel *in situ* synthesis technique. The unique dispersion technique led to nanocomposite films exhibiting exfoliated morphologies. High clay dispersion was indicated with the absence of XRD diffraction peaks, but exfoliation at low levels of clay loading was confirmed with TEM micrographs. The sonicated nanocomposites and CTAB-modified clay containing nanocomposites had predominately intercalated morphologies. The nanocomposites prepared through this *in situ* technique demonstrated lower WVT and WVP values compared with the sonication process. The incorporation of clay fillers increased the overall conversion of the nanocomposite systems up to 15%. The impact of clay loading on final nanocomposite film properties became evident with the trends observed with mechanical and thermal characterization. Introducing low levels of clay filler resulted in increased storage modulus, hardness, and thermal stability, but increasing the clay to higher concentrations diminished these properties. Additionally, optical clarity was shown to have a significant dependence on the volume of clay in each nanocomposite system as well as its dispersion.

The authors thank Scott Payne for his assistance with transmission electron microscopy and Brad Halverson for his assistance with X-ray diffraction measurements.

References

1. Gilman, J. W. Appl Clay Sci 1999, 15, 31.
2. Zhu, J.; Start, P.; Mauritz, K. A.; Wilkie, C. A. Polym Degrad Stab 2002, 77, 253.
3. Liu, T.; Ping Lim, K.; Chauhari Tjiu, W.; Pramoda, K. P.; Chen, Z.-K. Polymer 2003, 44, 3529.
4. Kawasumi, M.; Hasegawa, N.; Kato, M.; Usuki, A.; Okada, A. Macromolecules 1997, 30, 6333.
5. Tjong, S. Mater Sci Eng R Rep 2006, 53, 73.
6. Gilman, J. Chem Mater 2002, 14, 3776.
7. Choudalakis, G.; Gotsis, A. D. Eur Polym J 2009, 45, 967.
8. Cho, J.; Paul, D. Polymer 2001, 42, 1083.
9. Fischer, H. Mater Sci Eng C 2003, 23, 763.
10. Ray, S.; Okamoto, M. Progr Polym Sci 2003, 28, 1539.
11. Samyn, F.; Bourbigot, S.; Jama, C.; Bellayer, S.; Nazare, S.; Hull, R.; Fina, A.; Castrovinci, A.; Camino, G. Eur Polym J 2008, 44, 1631.
12. Paul, D.; Robeson, L. Polymer 2008, 49, 3187.
13. Meneghetti, P.; Qutubuddin, S. Thermochim Acta 2006, 442, 74.
14. Urresti, O.; González, A.; Fernández-Berridi, M. J.; Iruin, J. J.; Irusta, L. J Membr Sci 2011, 373, 173.
15. Herrera-Alonso, J. M.; Marand, E.; Little, J. C.; Cox, S. S. J Membr Sci 2009, 337, 208.
16. Bharadwaj, R. K.; Mehrabi, A. R.; Hamilton, C.; Trujillo, C.; Murga, M.; Fan, R.; Chavira, A.; Thompson, A. K. Polymer 2002, 43, 3699.
17. Swain, S. K.; Isayev, A. I. Polymer 2007, 48, 281.
18. Gorrasi, G.; Tortora, M.; Vittoria, V.; Pollet, E.; Lepoittevin, B.; Alexandre, M.; Dubois, P. Polymer 2003, 44, 2271.
19. Kim, J.-K.; Hu, C.; Woo, R. S. C.; Sham, M.-L. Compos Sci Technol 2005, 65, 805.
20. Picard, E.; Gérard, J. F.; Espuche, E. J Membr Sci 2008, 313, 284.
21. Giannakas, A.; Spanos, C. G.; Kourkoumelis, N.; Vaimakis, T.; Ladavos, A. Eur Polym J 2008, 44, 3915.
22. Weon, J. I.; Sue, H. J. Polymer 2005, 46, 6325.
23. Osman, M. A.; Mittal, V.; Lusti, H. R. Macromol Rapid Commun 2004, 25, 1145.
24. Frounchi, M.; Dadbin, S.; Salehpour, Z.; Noferesti, M. J Membr Sci 2006, 282, 142.
25. LeBaron, P. C.; Wang, Z.; Pinnavaia, T. J. Appl Clay Sci 1999, 15, 11.
26. Paul, M.-A.; Delcourt, C.; Alexandre, M.; Degée, P.; Monteverde, F.; Rulmont, A.; Dubois, P. Macromol Chem Phys 2005, 206, 484.
27. Usuki, A.; Kojima, Y.; Kawasumi, M.; Okada, A.; Fukushima, Y.; Kurauchi, T.; Kamigaito, O. J Mater Res 1993, 8, 1179.
28. Turner, S.; Matabayas, J. Polymer–Clay Nanocomposites; Wiley: Chichester, 2000, p 207.
29. Katoch, S.; Kundu, P. J Appl Polym Sci 2011, 122, 2731.
30. Zahouily, K.; Benfarhi, S.; Bendaikha, T.; Baron, J.; Decker, C. RadTech Eur, Basel, Switzerland, 2001, pp 583.
31. Zahouily, K.; Decker, C.; Benfarhi, S.; Baron, J. Radtech: The Premier UV/EB Conference and Exhibition, Indiannapolis, IN, April 28–May 1, 2002, pp 309.
32. Decker, C.; Zahouily, K.; Keller, L.; Benfarhi, S.; Bendaikha, T.; Baron, J. J Mater Sci 2002, 37, 4831.
33. Uhl, F. M.; Davuluri, S. P.; Wong, S.-C.; Webster, D. C. Polymer 2004, 45, 6175.
34. Li, F.; Zhou, S.; Wu, L. J Appl Polym Sci 2005, 98, 2274.
35. Uhl, F. M.; Webster, D. C.; Davuluri, S. P.; Wong, S.-C. Eur Polym J 2006, 42, 2596.
36. Lee, C.; Hall, H. K. Macromolecules 1989, 22, 21.
37. Ravindran, N.; Vora, A.; Webster, D. C. J Coat Technol Res 2006, 3, 213.
38. Ravindran, N.; Vora, A.; Webster, D. C. J Appl Polym Sci 2007, 105, 3378.
39. Kim, H. G.; Han, D. H.; Lim, J. C.; Oh, D. H.; Min, K. E. J Appl Polym Sci 2006, 101, 3609.
40. Curtis, L.; Edwards, D.; Simons, R.; Trent, P.; Von Bramer, P. Ind Eng Chem Prod Res Dev 1964, 3, 218.
41. Carothers, W. H.; Arvin, J. A. J Am Chem Soc 1929, 51, 2560.
42. Yang, Y. S.; Pascault, J. P. J Appl Polym Sci 1997, 64, 133.
43. Tolga, A. Nanocomposites based on recycled poly(ethylene terephthalate), M.S. Thesis, Middle East Technical University, 2005.
44. Uhl, F. M.; Davuluri, S. P.; Wong, S.-C.; Webster, D. C. Chem Mater 2004, 16, 1135.
45. Morgan, A. B.; Gilman, J. W. J Appl Polym Sci 2003, 87, 1329.
46. Ishida, H.; Campbell, S.; Blackwell, J. Chem Mater 2000, 12, 1260.
47. Leterrier, Y. Progr Mater Sci 2003, 48, 1.
48. Yeun, J.-H.; Bang, G.-S.; Park, B. J.; Ham, S. K.; Chang, J.-H. J Appl Polym Sci 2006, 101, 591.
49. Osman, M. A.; Mittal, V.; Morbidelli, M.; Suter, U. W. Macromolecules 2003, 36, 9851.
50. George, S. C.; Thomas, S. Progr Polym Sci 2001, 26, 985.
51. Miyagawa, H.; Rich, M. J.; Drzal, L. T. Polym Compos 2005, 26, 42.
52. Strawhecker, K.; Manias, E. Chem Mater 2000, 12, 2943.